Int J Earth Sci (Geol Rundsch) (2016) 105:2061–2073
DOI 10.1007/s00531-016-1372-6

ORIGINAL PAPER

Dextral strike-slip along the Kapıdağ shear zone (NW Turkey): evidence for Eocene westward translation of the Anatolian plate

Ercan Türkoğlu[1] · Gernold Zulauf[1] · Jolien Linckens[1] · Timur Ustaömer[2]

Received: 10 October 2015 / Accepted: 30 June 2016 / Published online: 11 July 2016

Abstract The northern part of the Kapıdağ Peninsula (Marmara Sea, NW Turkey) is affected by the E–W trending Kapıdağ shear zone, which cuts through calc-alkaline granitoids of the Ocaklar pluton resulting in mylonitic orthogneiss. Macroscopic and microscopic shear-sense indicators, such as SC fabrics, shear bands, σ-clasts and mica fish, unequivocally suggest dextral strike-slip for the Kapıdağ shear zone. Based on petrographic data, deformation microfabrics of quartz and feldspar, and the slip systems in quartz, the dextral shearing should have been active at T = 500–300 °C and P < 5 kbar. Published K–Ar and ^{39}Ar–^{40}Ar cooling ages of hornblende and biotite suggest that cooling below 500–300 °C occurred during the Eocene (ca. 45–ca. 35 Ma), meaning that the Kapıdağ shear zone should have been active during Middle to Late Eocene times. The differential stress related to the shearing was <50 MPa as is indicated by the size of recrystallized quartz grains. Based on the new and published data, it is concluded that the westward movement of the Anatolian plate might have been active almost continuously from the Middle Eocene until recent times.

✉ Ercan Türkoğlu
e.turkoglu@outlook.de

Gernold Zulauf
g.zulauf@em.uni-frankfurt.de

Jolien Linckens
linckens@em.uni-frankfurt.de

Timur Ustaömer
timur.ustaomer@gmail.com

[1] Institut für Geowissenschaften, Goethe Universität, Altenhöferallee 1, 60438 Frankfurt am Main, Germany

[2] Mühendislik Fakültesi, Jeoloji Mühendisliği Bölümü, İstanbul Üniversitesi, 34320 Avcılar-İstanbul, Turkey

Keywords Kapıdağ shear zone · North Anatolian fault · Marmara region · Strike-slip · Eastern Mediterranean

Introduction

The recent movement of lithospheric plates in the Eastern Mediterranean is dominated by counterclockwise rotation resulting in the westward translation of the Anatolian plate into the N–S extending Aegean domain (e.g., Le Pichon and Kreemer 2010, and references therein). The westward movement of the Anatolian plate is controlled by the dextral slip along the North Anatolian Fault (NAF), which splits into a northern and southern strand west of about 30.6° E. Extension in the Aegean domain is attributed to slab rollback and southward migration of the Hellenic subduction zone (Okay 2008) (Fig. 1). While the dextral slip along the NAF should have been active subsequent to the collision of the Anatolian and Arabian plates in the Miocene (Şengör et al. 2005), N–S extension in the Aegean domain (Cyclades, Menderes) is older and dates back at least to the Oligocene (e.g., Jolivet and Brun 2008). Given, there is a genetic link between the dextral movements in NW Anatolia and the N–S extension in the Eastern Mediterranean (Okay 2008), it is important to explore whether the dextral slip in NW Anatolia could have started earlier. Recent studies, which have focused on the kinematics and thermal evolution of E–W trending shear zones in SW Thrace and in the Uludağ Massif, suggest that the dextral slip along these shear zones commenced already in the Oligocene (Zattin et al. 2005; Okay et al. 2008). In the present paper, we will show that the dextral movements may have started even earlier during the Eocene when NW Anatolia was affected by pervasive magmatism. It commenced to be active following the collision of the Anatolide–Tauride

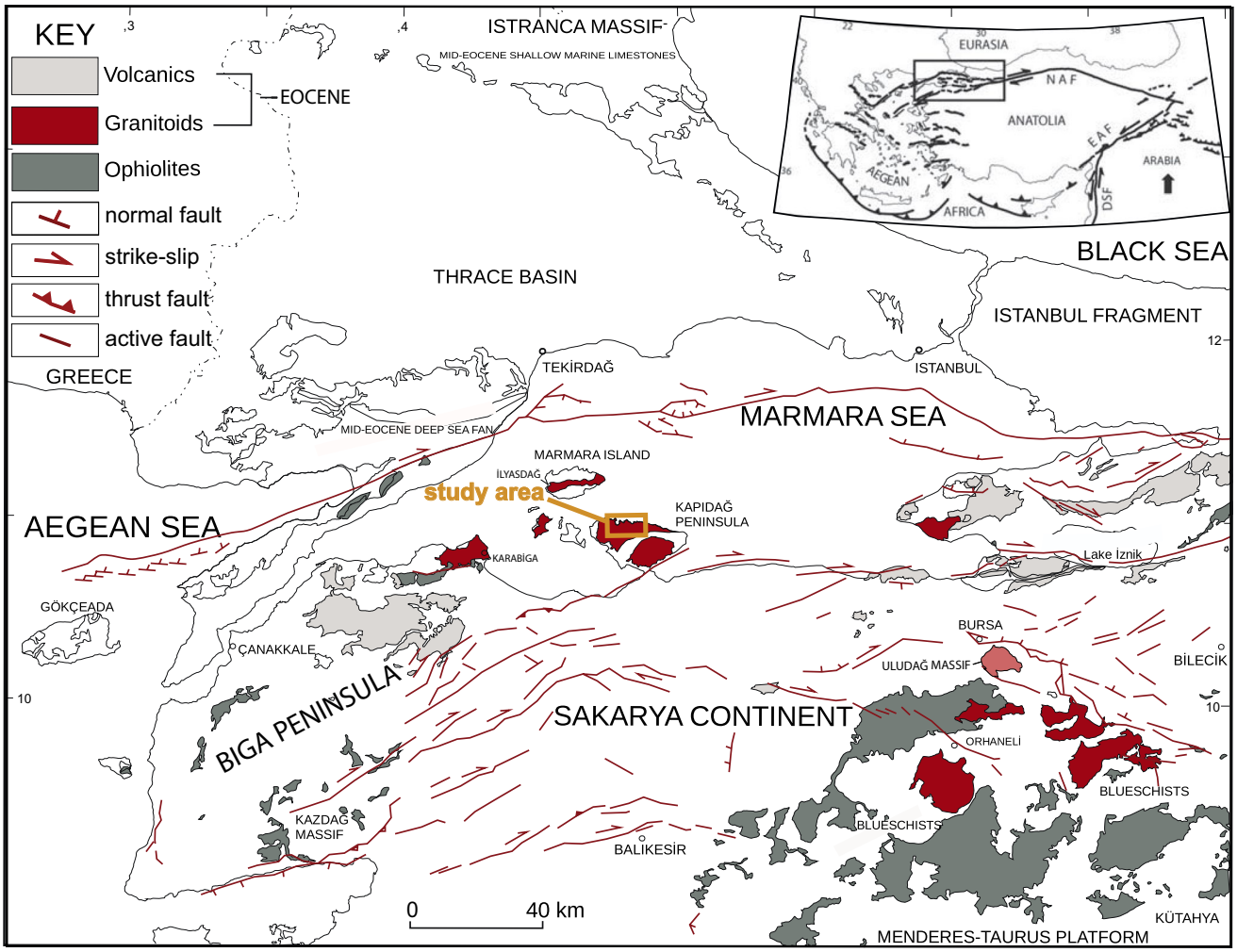

Fig. 1 Tectonic map of the Marmara region showing the distribution of Eocene magmatic rocks and of ophiolites (*inset* modified after Rockwell et al. 2009)

Platform with the Pontide arc along the Izmir–Ankara–Erzincan suture zone prior to the early Middle Eocene (e.g., Harris et al. 1994; Okay and Satır 2000).

We are focusing on the kinematics and thermal evolution of the Kapıdağ shear zone (Aksoy 1998), which cuts through the granitoids on the Kapıdağ Peninsula. This shear zone belongs to the E–W trending strike-slip shear zones, which follow the southern branch of the NAF in the Biga Peninsula (Fig. 1). The Kapıdağ shear zone is present in the northern part of the Kapıdağ Peninsula, where the Ocaklar granitoids were transformed into mylonitic gneisses (Fig. 2). Based on finite strain data and map-scale foliation pattern, Aksoy (1998) argued for a sinistral strike-slip of the Kapıdağ shear zone. The present study is focusing on the microfabrics, petrography and metamorphic index minerals of the mylonites of the Kapıdağ shear zone. The field work was carried out along the northern coast of the Kapıdağ Peninsula between Turan and Ormanlı (Fig. 2). The new data will be used to constrain the metamorphic temperature related to the shearing. Based on the temperature range, combined with published radiometric and fission-track ages, the timing of the mylonitic shearing of the Kapıdağ shear zone will be determined. The new data will show that the Kapıdağ shear zone does not result from sinistral, but from dextral strike-slip, that was active in Eocene times.

Geological setting

The Kapıdağ Peninsula consists of metamorphic rocks of the Erdek Complex, which have been intruded by the Ocaklar and the Çeltikçi Granitoid (Fig. 2). The metabasite-phyllite-marble sequence of the Erdek Complex underwent lower amphibolite- to greenschist facies metamorphism and is attributed to the Nilüfer Unit of the Permo–Triassic

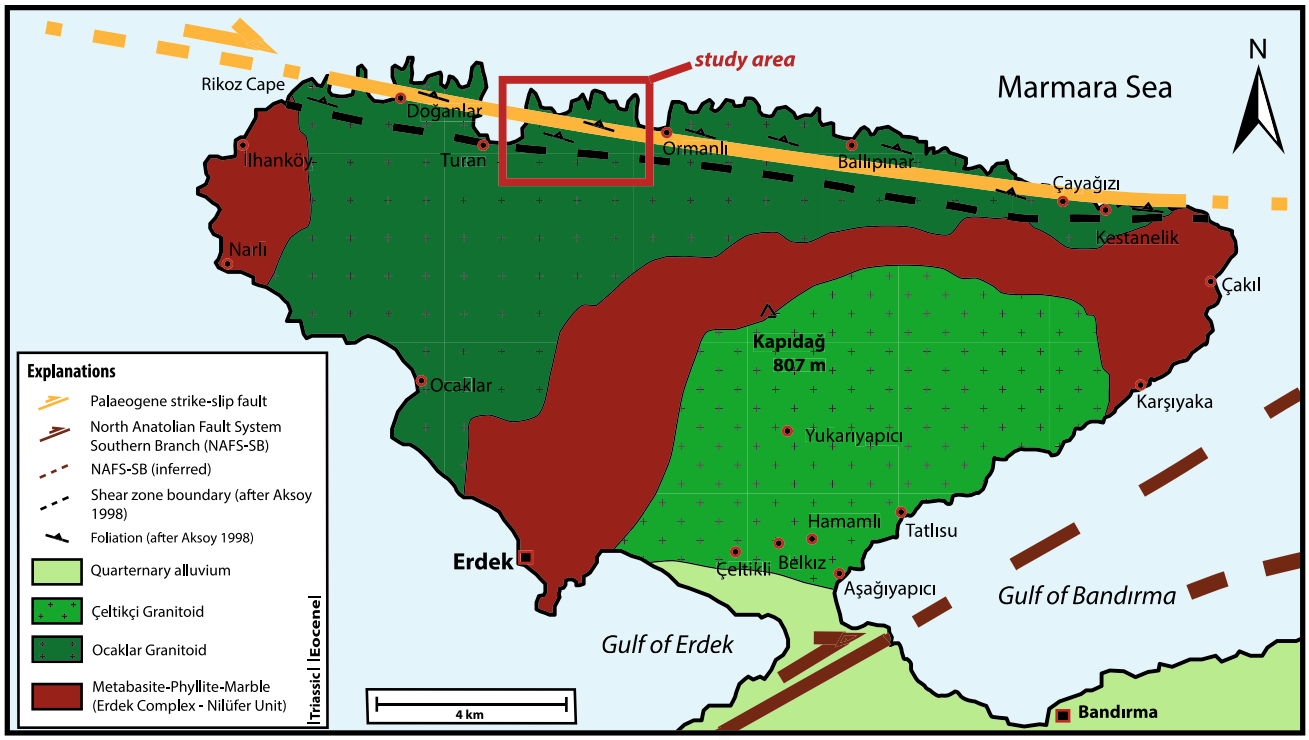

Fig. 2 Geologic map of the Kapıdağ Peninsula including data of Aksoy (1998)

Karakaya Complex (Aksoy 1996, 1998). The rocks of the Karakaya Complex were affected by deformation and metamorphism during late Triassic subduction and closure of Paleotethys (Okay and Göncüoglu 2004).

The Ocaklar and Çeltikçi granitoids belong to the magmatic belt of the northern Karakaya Complex, which is largely Eocene in age (Fig. 1; Bingöl et al. 1982; Delaloye and Bingöl 2000; Genç and Yılmaz 1997; Karacık et al. 2008; Köprübaşı and Aldanmaz 2004; Ustaömer et al. 2009). The Ocaklar pluton consists of medium to coarse-grained, leucocratic quartz diorite, tonalite and granodiorite (Sarialioglu 1983; Gözler et al. 1983; Aksoy 1996). In the sheared domains in the northern part of the Kapıdağ Peninsula, the granitoids are transformed into mylonitic orthogneisses, which show a similar composition like the protolith (Ketin 1946; Sarıalioğlu 1983). The main constituents are quartz, feldspar, biotite and amphibole. Accessories are muscovite, chlorite, epidote, apatite, titanite, orthite and opaque phases. The granitoids are cut by quartz, aplite and lamprophyre dikes, which are up to 80 cm in width. The gneissic rocks of the Ocaklar granitoids usually contain mafic enclaves, which have been used as strain markers and for constraining the kinematics of the Kapıdağ shear zone (Aksoy 1998).

U–Pb dating of zircons yielded 73.9 ± 8 Ma for the Ocaklar Granitoid (Bürküt 1966). This age, however, is not based on a robust analytical method, because Bürküt (1966) produced an arbitrary zircon standard himself and made a comparison with the sample from the Kapıdağ granitoid by pulverizing its containing zircons. For this reason, it is regarded as an unreliable age. K–Ar dating of hornblende and of biotite, separated from the Ocaklar granitoids, yielded 42.2 ± 1 Ma (hornblende) and 39.9 ± 0.8 and 38.3 ± 0.8 Ma (biotite) (Delaloye and Bingöl 2000).

The Çeltikçi granitoids to the south consist of diorite and hornblende–biotite granodiorite (Sarıalioğlu 1983; Aksoy 1996). The main phases are quartz, K-feldspar, plagioclase, hornblende, biotite and accessory sphene (Aksoy 1998). The Çeltikçi granitoids are frequently cut by aplite, pegmatite and quartz dikes. In contrast to the Ocaklar granitoids, there is no evidence for significant deformation in the Çeltikçi granitoids. U–Pb dating of zircon yielded 36.8 ± 0.7 (Altunkaynak et al. 2012). K–Ar dating of biotite yielded 38.2 ± 0.8 and 36.1 ± 0.8 Ma (Delaloye and Bingöl 2000).

The K–Ar ages mentioned above are cooling ages, which could be significantly younger than the emplacement age of the plutons. U–Pb zircon ages of the adjacent İlyasdağ pluton (Marmara Island) and Karabiga pluton (near Biga) yielded emplacement ages of 47.6 ± 2 Ma (Ustaömer et al. 2009) and 47.0 ± 1 Ma (Altunkaynak et al. 2012), respectively. Apatite fission-track ages obtained from granitoids of the southern part of the Kapıdağ Peninsula range from 28 ± 2 to 32 ± 2 Ma (Hejl et al. 2010).

The Kapıdağ shear zone, as mapped by Aksoy (1998) along the northern coast of the Kapıdağ Peninsula, extends almost E–W from Rikoz Cape in the west, via just south of Doğanlar, Turan, Ormanlı, Ballıpınar, Çayağzı and Kestanelik villages, toward the north of Çakıl village in the east (Fig. 2). The shear zone has a minimum thickness of 3.5 km and shows a gradational contact with the undeformed Ocaklar granitoid toward the south (Aksoy 1998).

Methods

The orientation of the mylonitic foliation and the mineral/stretching lineation of the orthogneisses in the Kapıdağ shear zone was measured in the field. Outcrop sections oriented perpendicular to the foliation and parallel to the lineation (*XZ* sections) were studied concerning the macroscopic sense of shear. Oriented samples of mylonites were collected from several outcrops for detailed analyses. Using thin sections (*XZ* sections) of these samples, the mylonites were studied concerning (1) the microscopic sense of shear, (2) the deformation microfabrics of the constituent minerals (quartz, feldspar, biotite, hornblende) and (3) metamorphic index minerals.

To reveal the active slip systems in quartz, three samples were examined using electron backscatter diffraction (EBSD). After performing petrographic analyses, thin sections were embedded in epoxy resin and then polished with colloidal silica on a vibratory polisher (SYTON method of Fynn and Powell 1979). Thin sections were coated with a thin layer of carbon and surrounded with a thin copper band in order to minimize ionic charging. EBSD analyses were conducted using a JEOL JSM 6490 scanning electron microscope (SEM) equipped with a HKL Nordlys EBSD detector. Acceleration voltage for the measurements was 15 kV, beam current was ~8 nA and the working distance between 17 and 20 mm. EBSD patterns were indexed using the HKL Technology Channel 5 software (Schmidt and Olesen 1989). Only EBSD measurements with a mean angular deviation (MAD) of <1.3 were accepted and recorded. Maps were generated using a step size of 6 µm. Pole figures with one *c*-axis orientation per grain were plotted as lower hemisphere, equal-area projections.

To determine the differential stress (σ_1–σ_3) related to the most important and pervasive deformation event, we used a paleopiezometer that is based on the dynamically recrystallized grain size of quartz. Twiss (1977) has shown the following relation between the stress difference and the recrystallized grain size:

$$(\sigma_1 - \sigma_3) = K\mu B d^{-r}$$

where μ is the shear modulus, B is the Burgers vector, and K and r are empirically derived constants (cf. also Twiss and Moores 1992, p. 412). Main prerequisites for the application of the recrystallized grain-size piezometer are: (1) the growth of the recrystallized grains should not be influenced by other phases, (2) the recrystallized grains must reflect a steady-state deformation and (3) grain growth due to static annealing should not occur subsequent to the formation of the recrystallized grains. In the present case of the Kapıdağ samples, the type of quartz recrystallization is difficult to constrain. There is evidence for grain-boundary migration, but because of similar size of subgrains and recrystallized grains, subgrain rotation should also have contributed to the recrystallization. Apart from the theoretical calibration of Twiss (1977),

As most of the grains show irregular shapes, we determined the diameter from the grain area that was measured using an image-analyses system. For every sample, at least 25 grains were analyzed to calculate the mean grain size and the standard deviation.

Results

Structural record in the field

The study area consists of the Ocaklar granitoid, which shows significant changes in the degree of deformation and finite strain. The less deformed, almost intact Ocaklar granitoid is exposed ca. 2 km south of the coastline between Turan and Ormanlı (Fig. 2). Toward the north, the granitoid is progressively sheared and deformed into mylonitic orthogneiss. The foliation of this orthogneiss is pervasive and results from the shape-preferred orientation of the constituent minerals, mainly plagioclase, quartz and biotite. The mylonitic lineation is portrayed by biotite and stretched quartz and feldspar. The orientation of the foliation and of the mineral/stretching lineation is depicted in Figs. 3, 4 and 6. The foliation of the mylonitic orthogneiss dips toward NNE to NE with varying dip angle. Most of the foliation planes show almost pure strike-slip lineations (Figs. 3, 4). Most variations in the attitude of the foliation are present in the margins of the shear zone strike where the strain magnitude is moderate to weak. The attitude of the foliation is strong along the coastline, particularly between the Manastır beach and the coast of Hiliköy Koyu with a dip angle between 70° and 78° (Fig. 3). The northern margin of the shear zone strike is offshore (Aksoy 1998). There are a large number of mafic enclaves within the orthogneiss (Fig. 5). In high-strain domains, these enclaves are strongly elongated, with their long axes oriented parallel to the subhorizontal mineral/stretching lineation of the metagranitoid host. The mean orientation of the long axis of the deformed mafic enclaves is N 80°–90° W (Aksoy 1998: Fig. 7).

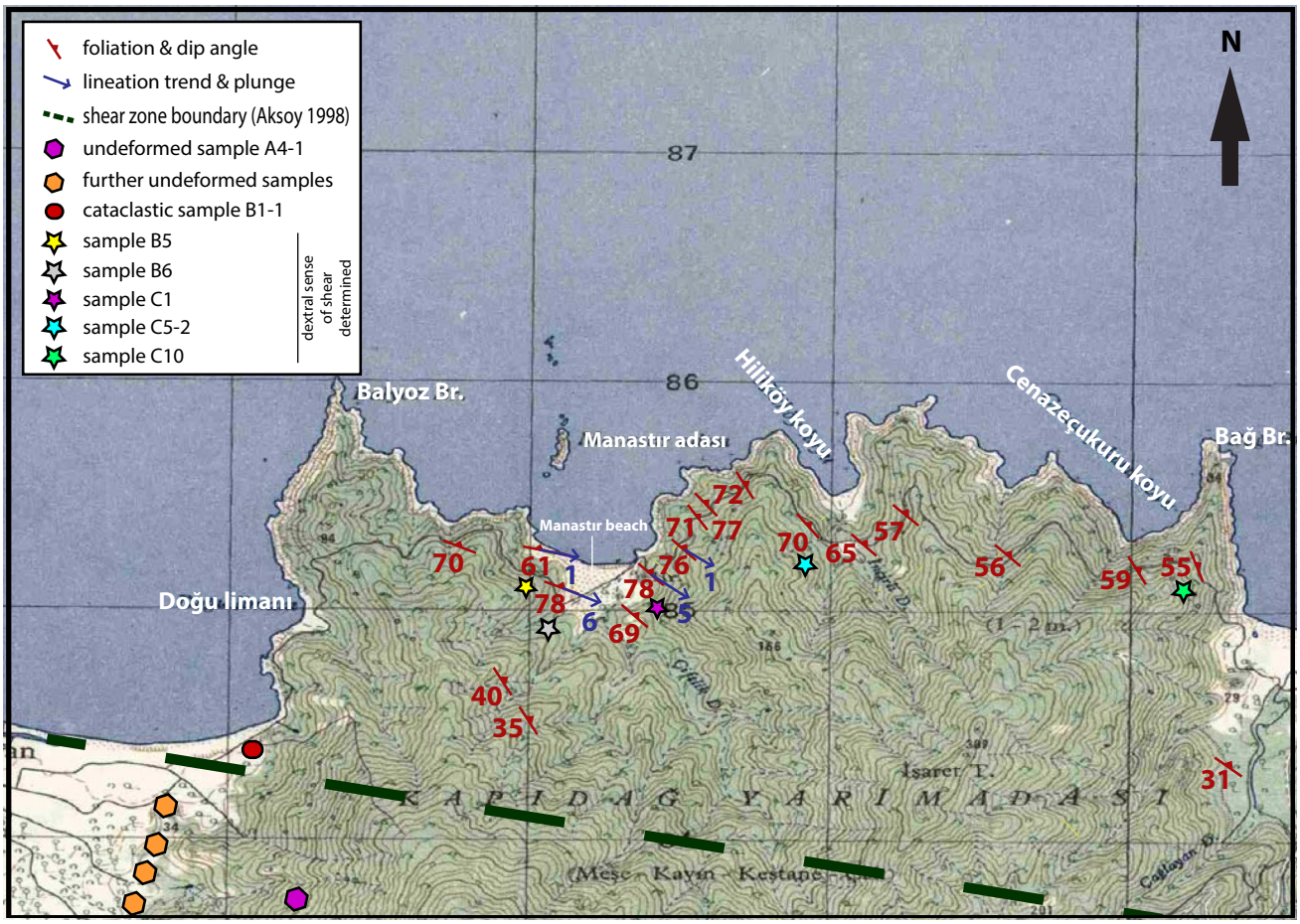

Fig. 3 Structural data obtained in the study area between Turan and Ormanlı. Sample locations indicate the obtained shear-sense data. 1:25,000 map scale

Asymmetric fabrics in outcrop sections oriented perpendicular to the foliation and parallel to the mineral/stretching lineation suggest non-coaxial deformation. SC fabrics and asymmetrically shaped σ-type clasts of feldspar indicate a dextral sense of shear (Fig. 6).

At a few places only, the steep strike-slip foliation cuts through an older widely spaced, discrete foliation, which is subhorizontal or only moderately inclined (Fig. 5). The kinematics of this fabric, however, is difficult to constrain from macroscopic observations. There are also places, where crosscutting relationships between both fabrics are not clear, and sometimes the discrete planes look like joints.

Petrography and microfabrics

Low-strain domains

The low-strain granitoids have only been found south of the shear zone boundary, mapped by Aksoy (1998) (Figs. 2, 3). They consist of the primary magmatic minerals, quartz, plagioclase, K-feldspar, biotite and hornblende (Fig. 7a). These minerals are up to 7 mm in size and do not show a shape-preferred orientation. The microfabrics of the low-strain domains reveal weak deformation of the Ocaklar granitoid (Fig. 7b). Quartz shows undulatory extinction and in a few cases serrated grain boundaries, which result from bulging (Fig. 7b). Plagioclase shows optical zonation and magmatic twins. Biotite is sometimes kinked. Transgranular fractures are common.

High-strain domains

The mylonitic orthogneisses of the high-strain domains are characterized by a shape-preferred orientation of the constituent minerals and by a reduction in grain size. The average grain size of the rocks is 1–2 mm. The grain size decreases along the shear zone boundary from west to east of the study area. Apart from the primary magmatic minerals, the high-strain domains include accessory minerals like white mica, epidote, apatite, chlorite and orthite, which result from fluid-controlled metamorphic reactions during

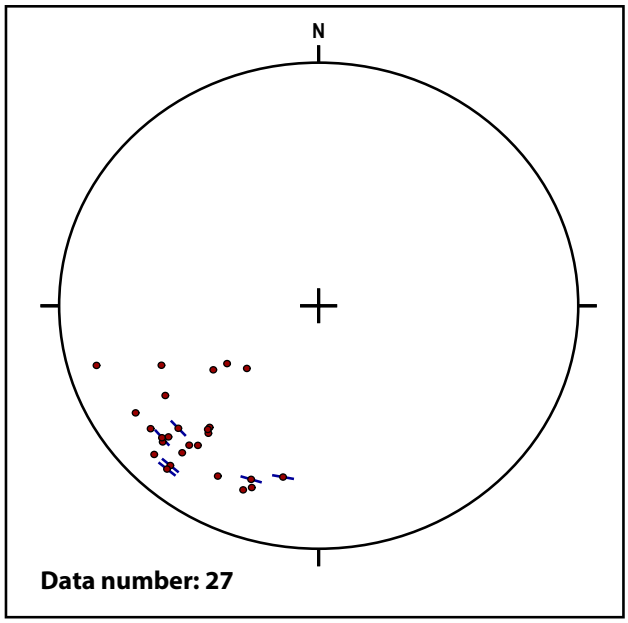

Fig. 4 Structural data plotted in equal-area lower-hemisphere projection. Poles to mylonitic foliation (*red*) with related stretching lineation (*blue*) are plotted after method of Hoeppener (1955)

the shearing (see also Aksoy 1998). The long axis of biotite is frequently oblique with respect to the mylonitic foliation. These biotite fishes are portraying the S-planes of SC fabrics, which indicate a dextral sense of shear (Fig. 8c, d). A dextral sense of shear is also indicated by shear bands and by σ-clasts of feldspar, which result from asymmetric pressure shadows of recrystallized quartz behind the rigid feldspars.

Large magmatic relicts of quartz show undulatory extinction and/or subgrains (Fig. 8f). Quartz, however, is in most cases completely recrystallized (Fig. 8c, d). The size of the recrystallized grains is similar to the size of some of the subgrains, with a maximum value of ca. 300 µm. Recrystallized grain-size statistics of two samples (each 25 grains) yielded 193 ± 112 and 73 ± 21 µm. These values result in a paleodifferential stress of 19 + 15/−5 MPa and 37 + 10/−6 MPa, respectively, when using the theoretical parameters of Twiss (1977). EBSD analyses obtained from sample B6 yielded a single girdle of quartz c-axes indicating rhombohedral slip and prism <a> slip (Passchier and Trouw 2005; Fig. 9). EBSD analyses obtained from sample C5-2 yielded a pattern of quartz c-axes, which indicates a transition between a single and crossed girdle (Fig. 9), where one side of the crossed girdle is much more pronounced than the other. This pattern indicates basal, prism and rhomb <a> slip. Sample C10 yields a relict crossed girdle, which shows a narrow opening angle (Fig. 9). This pattern also indicates the activity of basal, prism and rhomb <a> slip, with a bigger contribution of basal <a> slip than in sample C5-2. The asymmetry of the

Fig. 5 Deformed mafic enclaves inside mylonitic metagranitoid with their long axes oriented parallel to the NNE-dipping mylonitic foliation; Manastır beach

Fig. 6 S-C fabric in mylonite of the Ocaklar metagranitoid indicating dextral strike-slip; Manastır beach

quartz c-axes is not clear and has not been used to constrain the sense of shear.

Magmatic plagioclase is largely preserved but strongly deformed. Deformation of plagioclase is indicated by undulatory extinction, fractures, subgrains, deformation twins (according to the albite and pericline law) and bending of twins (Fig. 8e). In few cases, there is evidence for incipient recrystallization along the grain margins in form of many new small grains, the latter with sizes around 0.05 mm (Fig. 8b). Magmatic oscillatory zonation of plagioclase is also preserved (Fig. 8c, left part). In many cases, the anorthite-rich central parts of the plagioclases are strongly sericitized or replaced by other tiny minerals, such as epidote, titanite ('filled plagioclase'). The samples B5 and B6, which contain metamorphic index minerals like epidote and titanite, are delivered from the Manastır beach (see Fig. 3). K-feldspar is affected by dissolution of albite resulting in flame perthite (Fig. 8a). Brittle deformation of plagioclase during the late kinematics is indicated by open fractures, which are filled with quartz (Fig. 8e).

Magmatic biotite shows undulatory extinction, bending, kinking and fracturing (Fig. 8c, d). The asymmetric shape of many biotites results in biotite fishes, which indicate a dextral sense of shear (Fig. 8c, d). Some of these biotite fishes show pressure shadows filled with newly grown epidote.

Magmatic hornblende is deformed by brittle fracturing, accompanied by strong grain-size reduction if strain is significant.

There are discrete zones inside the mylonites described above, which show a higher number of cataclastic fabrics and retrograde metamorphism. These zones are characterized by solution-precipitation creep of fine-grained quartz, and fracturing of almost all minerals. There is further evidence for the formation of chlorite and white mica (sericite) at the expense of biotite and feldspar.

Discussion

The new data presented above can be used to constrain the sense of shear, the thermal conditions and the differential stress related to the movements along the Kapıdağ shear zone. Moreover, combining these data with published radiometric ages, we can constrain the period during which the dextral slip along the Kapıdağ shear zone occurred.

Kinematics

The subhorizontal mineral/stretching lineation on N- to NE-dipping mylonitic foliation planes clearly confirm the view of Aksoy (1998) that we are dealing with a strike-slip shear zone, which cuts through the Ocaklar pluton. The kinematics of this shear zone is shown by different types of shear-sense indicators, which are present both macroscopically and microscopically. SC and shear-band fabrics, biotite fish and σ-clasts of feldspar unequivocally indicate

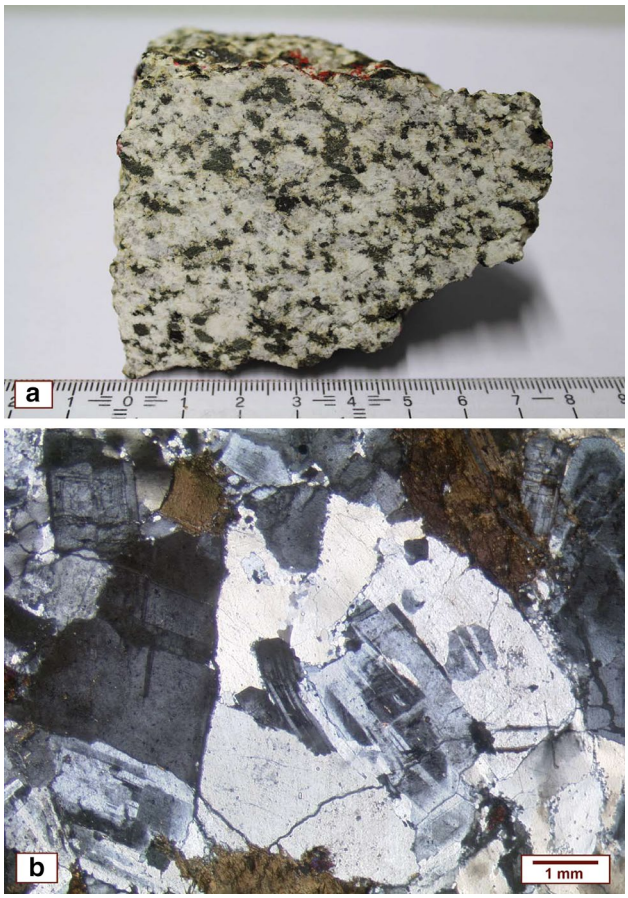

Fig. 7 Sample A4-1 of largely undeformed Ocaklar granitoid, collected near Turan, is shown macroscopically (**a**), and microscopically with crossed polarizers (**b**)

a dextral sense of shear, which, however, is not consistent with the sinistral kinematics derived by Aksoy (1998). There are several reasons, why the sinistral kinematics is not reliable: (1) No macroscopic shear-sense indicators have been presented by Aksoy (1998); (2) microscopic and microfabric studies in particular have not been carried out; (3) the map-scale foliation pattern used by Aksoy (1998) to determine a sinistral sense of shear is not robust, because mesoscale and microscopic kinematic indicators in the study area argue for a dextral sense of shear. The kinematic significance of the discrete low-angle foliation, which largely pre-dates the steeper, and pervasive strike-slip foliation is yet not clear and needs further investigations.

Thermal and stress conditions

The new data presented above can be used to better constrain the temperature range during which the deformation of the Ocaklar granitoid occurred. The following observations are important: (1) apart from local replacement by chlorite along discrete shear planes, biotite was largely

Fig. 8 Microphotographs of deformed Ocaklar metagranitoid under crossed polarizers. Foliation is perpendicular to the lineation, whereas the lineation is parallel to the long side of the microphotographs. **a** Flame perthite in microcline. Incipient recrystallization of feldspar at upper grain margin. Biotite is partly replaced by chlorite and epidote. Quartz is completely recrystallized. Sample: B5, location: near Manastır beach. **b** Recrystallized grains of plagioclase are significantly smaller than recrystallized grains of quartz. Sample: C5-2, location: Manastır beach. **c** Biotite fish with deflected cleavage indicating dextral shear sense. Note epidote grains in tailed area. Quartz of the matrix is pervasively recrystallized. Plagioclase shows optical zonation, deformation twins and in some cases evidence for bulging. Sample: B6, location: Manastır beach. **d** Elongated and strongly altered biotite fish in recrystallized quartz matrix indicates dextral shear sense, which is also shown by shear bands. Magmatic plagioclase shows kinking and deformation twins. Sample: C5-2, location: Manastır beach. **e** Large magmatic plagioclase shows deformation twins (according to the albite and pericline law) as well as an extension fracture that is filled with quartz. Recrystallization of the large plagioclase starts in the lower part of the crystal. Both plagioclase and biotite are partly replaced by epidote. Biotite is strongly bent. Sample: C10, location: near Ormanlı. **f** Brittle–ductile shear zone exposed near Turan (sample B1-1). Quartz shows fracturing, subgrains and recrystallized grains. Biotite is characterized by undulatory extinction and slight bending. Feldspar is strongly altered in form of sericitization

stable during shearing; (2) igneous chemical zonation in plagioclase is largely preserved; (3) plagioclase is fractured, kinked and mechanically twinned; in few cases it shows evidence for incipient recrystallization; (4) K-feldspar is partly replaced by albite resulting in flame perthite; (5) all feldspars are more or less affected by alteration in form of replacement by secondary minerals, such as sericite, epidote; (6) most of the quartz is recrystallized by strain-induced grain-boundary migration and by subgrain rotation, the latter indicated by the similar size of recrystallized grains and some of the subgrains.

The microfabrics of plagioclase (incipient recrystallization, deformation twins, fracturing) and the formation of flame perthite suggest deformation temperatures between 400 and 500 °C (Passchier and Trouw 2005, and references therein). This range is consistent with the stability of biotite and with the growth of epidote. High fluid-rock ratios, decreasing temperatures and retrograde metamorphism to lower greenschist facies conditions are documented by the formation of chlorite at the expense of biotite and by sericitization of feldspar.

Thus, most of the finite strain of the Kapıdağ shear zone should have been accommodated under greenschist facies conditions between ca. 500 and 300 °C. This temperature interval is consistent with the slip systems (prism, rhombohedral and basal <a> slip) obtained from the quartz textures.

The pressure related to this temperature interval, however, is difficult to constrain. Based on the Al content of hornblende, Köprübaşı and Aldanmaz (2004) calculated

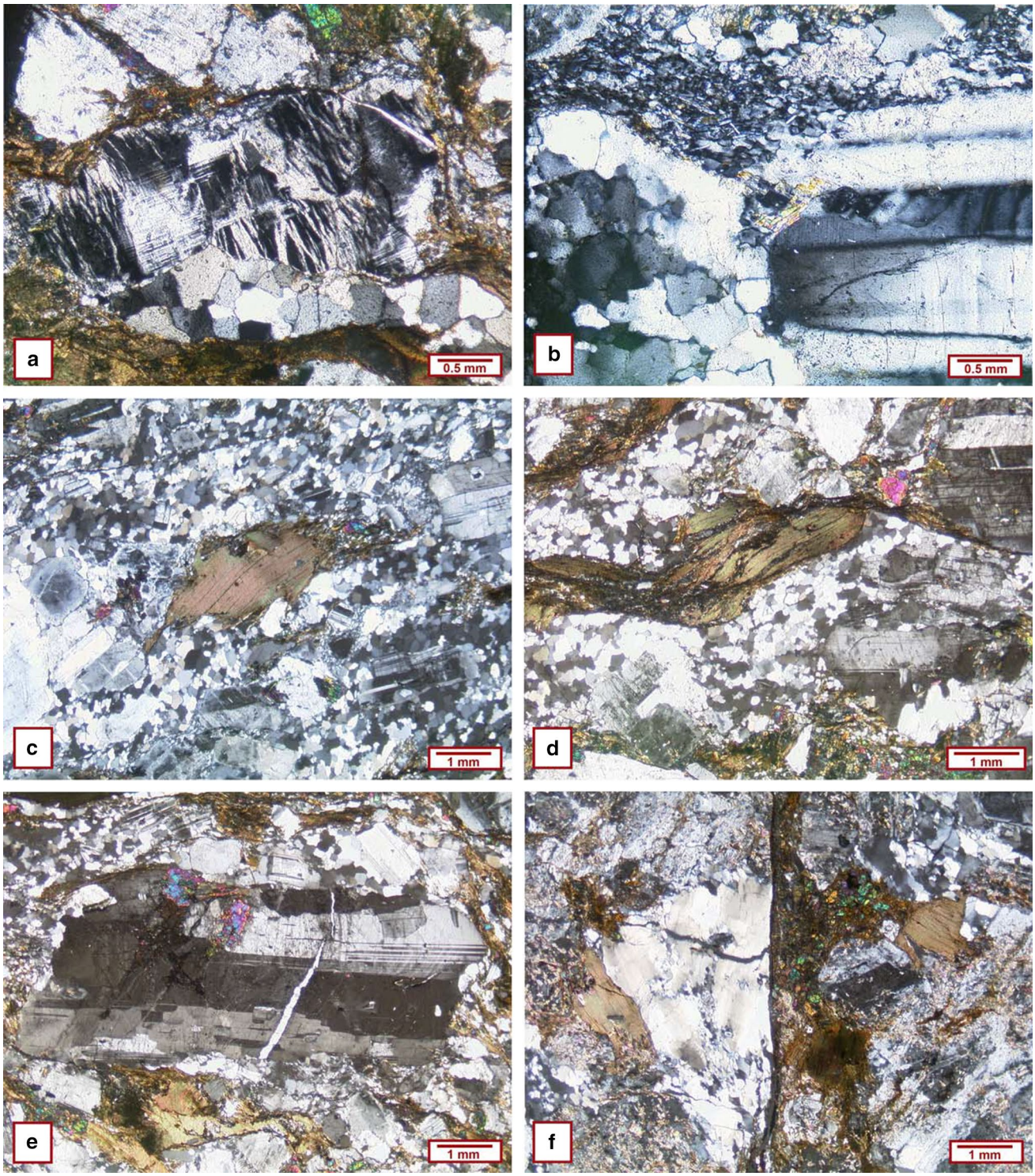

an emplacement depth of ca. 22 km for the Ocaklar pluton corresponding to a pressure of 5.8 ± 0.6 kbar. When assuming a common geothermal gradient in a collisional domain (30 ± 5 °C/km), this depth corresponds to a temperature of ca. 640 ± 100 °C. Thus, at least amphibolite-facies conditions should have been present in the host rock during melt emplacement. This assumption is compatible with the metamorphic imprints of the Erdek Complex, from which Aksoy (1996, 1998) described polyphase deformation under lower amphibolite to epidote–amphibolite facies conditions followed by retrograde metamorphism until the lower greenschist facies.

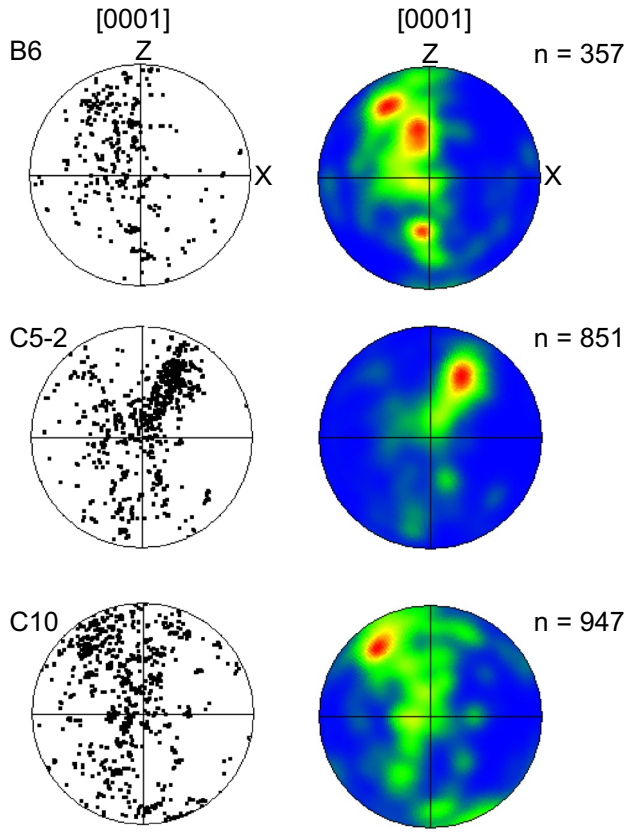

Fig. 9 Equal area, lower-hemisphere pole diagrams of quartz c-axes distribution based on electronic backscatter diffraction images of samples B6, C5-2 and C10 along the *c*-axis [0001]. *Left* one point per grain pole figures; *right* contoured pole figures

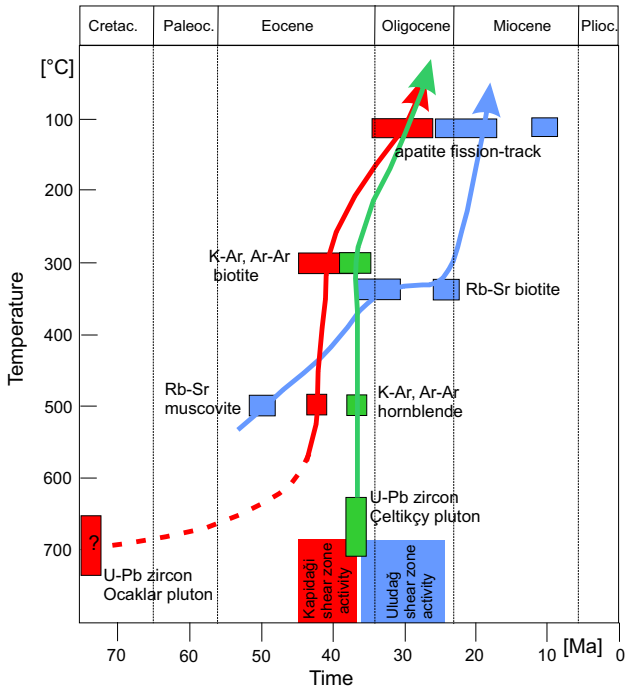

Fig. 10 Temperature–time–depth diagram showing the thermal evolution of the Ocaklar pluton (*red line*), Çeltikçi pluton (*green line*) and Uludağ massif (*blue line*, after Okay et al. and references therein). Radiometric cooling ages, see text. The ages of shearing of the Kapıdağ and Uludağ shear zones are indicated

The differential stress obtained from recrystallized grain size of quartz (<50 MPa) is in line with published data. On Evia island (Hellenides), Alpine deformation took place under ductile conditions (T = 450–500 °C) at differential stresses of 65 + 15/−10 MPa (Chatzaras et al. 2012). In the Cycladic Massif of Iraklia and Schinoussa islands, deformation in a subduction-related setting took place at T = 400–450 °C under differential stresses around 28–62 MPa (Behrmann and Seckel 2007). In the Bohemian Massif, Variscan deformation of metagreywackes at upper greenschist to lower amphibolite facies (Barrovian-type) conditions was active at differential stresses of ca. 20 MPa (Zulauf 2001).

Timing of shearing and regional implications

When taking the above temperature range (500–300 °C) into account, published radiometric ages could help to constrain the time window during which the shearing along the Kapıdağ shear zone occurred.

An upper age limit for the shearing is given by the age of the Ocaklar pluton. U–Pb dating of zircon yielded 73.9 ± 8 Ma, which could be interpreted as intrusion age (Bürküt 1966). Similar intrusion ages have been recently obtained for Asterousia-type granitoids exposed on Crete (Kneuker et al. 2014) and on Anafi (Martha et al. 2016). These rocks, however, are attributed to the Pelagonian Unit of the Internal Hellenides. The (meta)granitoids of NW Turkey, on the other hand, are Cenozoic in age and intruded during three distinct periods: (1) Early to Late Eocene, (2) Late Oliocene to Middle Miocene and (3) Late Miocene to Quaternary (Altunkaynak et al. 2012, and references therein). In the westernmost Pontides and the Biga peninsula, Eocene plutons are dominant. The Karabiga pluton of the Biga peninsula yielded a U–Pb zircon SHRIMP age of 47.02 ± 0.82 Ma, which is interpreted as emplacement age (Altunkaynak et al. 2012). The same U–Pb zircon age yielded the İlyasdağ granodiorite on Marmara island (47.6 ± 2 Ma; Ustaömer et al. 2009). As the composition of these granitoids is similar to that of the Ocaklar granitoid, it is possible that the Upper Cretaceous U–Pb age determined for the Ocaklar granitoid is wrong, and the real emplacement age is close to that of the Karabiga and İlyasdağ plutons, respectively. This assumption is supported by the fact that the analysis carried out by Bürküt (1966) is not robust compared with modern techniques (see above).

K–Ar dating of hornblende, separated from the Ocaklar granitoid, yielded 42.2 ± 1 Ma (Delaloye and Bingöl 2000). As the closure temperature for the K–Ar system of hornblende should be 530 ± 40 °C (Harrison 1981), the Ocaklar granitoid should have cooled below this temperature at ca. 42 Ma (Fig. 10). K–Ar dating of biotite of the Ocaklar granitoid yielded 39.9 ± 0.8 and 38.3 ± 0.8 Ma (Delaloye and Bingöl 2000), whereas recent Ar–Ar dating of biotite yielded 45.3 ± 0.1 Ma (Altunkaynak et al. 2012). The closure temperature for the K–Ar system of biotite has been constrained at 310 ± 30 °C (Harrison et al. 1985). For this reason, the biotite age should be lower than the hornblende age mentioned above. However, in the present case, the ^{39}Ar–^{40}Ar biotite age exceeds the K–Ar age of hornblende within the uncertainty of the ages. Thus, either the K–Ar hornblende or the ^{39}Ar–^{40}Ar biotite age is wrong. Another explanation for the misfit in cooling ages could be the adjacent Çeltikçi granitoid, which should be younger and different in composition compared to the Ocaklar granitoid (Aksoy 1998; Altunkaynak et al. 2012). U–Pb dating of zircon yielded 36.8 ± 0.7 Ma, which is interpreted as emplacement age (Altunkaynak et al. 2012; Fig. 10). K–Ar dating of biotite yielded 38.2 ± 0.8 and 36.1 ± 0.8 (Delaloye and Bingöl 2000). The thermal imprint of the Çeltikçi granitoid may have disturbed the isotopic systems of hornblende and of biotite inside the Ocaklar granitoid resulting in resetted and thus younger cooling ages. As the U–Pb zircon and the K–Ar biotite ages are almost the same, the Çeltikçi granitoid should have cooled very rapidly after melt intrusion pointing to a very shallow upper crustal emplacement level (<10 km), which is much shallower than the 22-km emplacement depth obtained for the Ocaklar granitoid (see above). Moreover, as the Çeltikçi and Ocaklar granitoids are in the same structural position at present, the Ocaklar granite must have reached the shallow crustal levels already at ca. 35 Ma.

As the emplacement age of the Ocaklar granitoid is not well constrained, we do not know how long the pluton was situated at deep crustal levels. However, the microfabrics suggest that the dextral shearing of the Kapıdağ shear zone commenced at T = ca. 500 °C and thus after significant cooling of the pluton. According to the radiometric cooling ages listed above, T = ca. 500 °C was attained at ca. 42 Ma or even somewhat earlier. Thus, the Kapıdağ shear zone should have been initiated at ca. 42 Ma. Most of the viscous strain inside the Kapıdağ shear zone was accommodated under greenschist facies conditions until T = ca. 300 °C was reached. According to the K–Ar and ^{39}Ar–^{40}Ar ages of biotite, the temperature was dropping down below ca. 300 °C at ca. 38 Ma or even earlier. This age corresponds to the emplacement age of the post-kinematic Çeltikçi granitoid. Thus, the main slip along the viscous Kapıdağ shear zone did not occur during the Oligocene, as assumed by Okay et al. (2008), but is constrained to the Middle to Upper Eocene (ca. 45–ca. 35 Ma; Fig. 10), which is consistent with assumptions made by Aksoy (1998).

Apatite fission-track ages obtained from the southern Kapıdağ Peninsula (30.6 ± 1.9 and 31.6 ± 2.0 Ma; Hejl et al. 2010) are similar to those determined from the Marmara island (31–23 Ma; Hejl et al. 2010). Thus, in the Oligocene, the rocks exposed today in the study area and surroundings should have been situated at uppermost structural levels where T < ca. 100 °C (Fig. 10). This shallow level is consistent with the fact that the rocks of the Izmir–Ankara–Erzincan suture zone (IAEZ), such as the Bornova flysch, were unconformably covered by continental to shallow marine sediments of Middle Eocene age (Yılmaz et al. 1997). The Middle to Late Eocene continental to shallow marine sediments are also exposed in the nearby regions of the Kapıdağ Peninsula. Note that the shallow marine sediments pass upward into turbidities with exotic blocks of various composition in the Late Eocene. The Eocene basin is filled by continental clastics of Late Eocene–Oligocene age with intercalations of intermediate to felsic lavas and tuffs.

The IAEZ reflects the late Cretaceous to early Eocene closure of the northern branch of the Neotethys due to the collision of the Sakarya/Pontide block with the Anatolide–Tauride Platform (e.g., Şengör and Yılmaz 1981; Okay and Tüysüz 1999). Consequently, apart from the Eocene emplacement of calc-alkaline granitoids, the Eocene dextral shearing along E–W trending strike-slip faults occurred in a post-collisional setting (Harris et al. 1994; Köprübaşı and Aldanmaz 2004; Altunkaynak et al. 2012).

A Middle to Late Eocene age for the dextral strike-slip of the Kapıdağ shear zone is consistent with radiometric ages of illite, which formed inside the NAF. Results of K–Ar dating of illite from the fault rocks of the NAF indicate that major faulting was initiated in the Paleocene at ~57 Ma (Uysal et al. 2006).

Ductile strike-slip along E–W trending crustal-scale shear zones did not stop during the Eocene in NW Anatolia but continued to be active further to the east in the Uludağ Massif. In this area, strike-slip along a 225-km-long WNW–ESE trending shear zone should have been active from Late Eocene to Oligocene (38–27 Ma) accommodating a dextral displacement of ca. 100 km (Okay et al. 2008). Granites intruded syn- and post-kinematically with respect to the shearing events (Okay et al. 2008). In contrast to the Kapıdağ Peninsula, the Uludağ Massif was exhumed much later as is indicated by apatite fission-track ages of 20–21 Ma (Okay et al. 2008). This late exhumation explains the ductile (viscous) behavior of the sheared rocks, although the shearing is Oligocene in age.

A Late Oligocene age for strike-slip movement along the NAF has been documented by electron spin resonance ages of quartz and by K–Ar dating of illite separated from fault gouge (Ulusoy 2004; Uysal et al. 2006). Zattin et al. (2005) found evidence for Late Oligocene and Middle Miocene activity along the NAF (Ganos fault) in southwestern Thrace. As the dextral slip of the active NAF should have started during the late Miocene (Şengör et al. 2005), dextral strike-slip along E–W trending faults was active in NW Anatolia almost continuously from the Middle Eocene (Kapıdağ) via the Oligocene and Miocene (Uludağ, Thrace) until recent. Consequently, the westward translation of the Anatolian microplate should have been active during the same time.

Based on a low-velocity band beneath the NAF, Fichtner et al. (2013) argue that the recent NAF is not only a crustal feature, but a narrow zone of weakness that extends into the upper mantle. It is not clear, however, whether this situation also holds for the southern branch of the NAF (Kahraman et al. 2015). Irrespective of the recent conditions at deeper structural levels of the NAF, the results of the present study reflect the deformation mechanisms and stress conditions of an infrastructural section of a shear zone, which might belong to an Eocene–Oligocene precursor of the NAF. These data give insights how deformation is focused at mid to lower crustal levels of the recent NAF.

Conclusions

Based on the new and published data, the following conclusions can be drawn:

- The Kapıdağ shear zone is part of a dextral E–W trending strike-slip zones that was active under greenschist facies conditions during the Middle to Late Eocene.
- Dextral strike-slip in NW Anatolia commenced probably earlier than previously assumed. It might have started during the Middle Eocene (or even earlier) and was active almost continuously during the Oligocene/Miocene (Uludag Massif; Thrace) until recent times (active NAF).
- Continuous N–S shortening of Anatolia, subsequent to the Late Cretaceous/early Cenozoic closure of the Neotethys, was accommodated by lateral escape and dextral strike-slip in NW Anatolia and related westward movement of the Anatolian plate.
- Although not verified by the recent studies, the close relation between intrusions and dextral shear zones in NW Turkey suggests a genetic link between both. It is possible that the intruded melts formed mechanically weak domains, where dextral strike-slip was initiated. Further studies are required to verify this hypothesis.

Acknowledgments This study has been supported by grants from the 'Freunde und Förderer der Goethe-Universität' and made possible by the partnership with the Department of Geology, Istanbul University, which are gratefully acknowledged. We thank H. Koral and two anonymous referees for their helpful comments.

References

Aksoy R (1996) Mesoscopic tectonic features of the Marmara island and the Kapıdağı peninsula, NW Turkey. Turk J Earth Sci 5:187–195

Aksoy R (1998) Strain analysis of the Kapıdağ Peninsula shear zone in the Ocaklar Granitoid, NW Turkey. Turk J Earth Sci 7:79–85

Altunkaynak S, Sunal G, Aldanmaz E, Genç CS, Dilek Y, Furnes H, Foland KA, Yang J, Yıldız M (2012) Eocene granitic magmatism in NW Anatolia (Turkey) revisited: new implications from comparative zircon SHRIMP U–Pb and 40Ar–39Ar geochronology and isotope geochemistry on magma genesis and emplacement. Lithos 155:289–309

Behrmann JH, Seckel C (2007) Structures, flow stresses, and estimated strain rates in metamorphic rocks of the Small Cyclades Islands Iraklia and Schinoussa (Aegean Sea, Greece). Geotecton Res 95:1–11

Bingöl E, Delaloye M, Ataman G (1982) Granitic intrusions in western Anatolia, a contribution to the geodynamic study of this area. Eclogae Geol Helv 75:437–446

Bürküt Y (1966) Batı Anadolu'da yeralan plütonların mukayeseli jenetik etüdü. ITÜ Maden Fak. yayını, Istanbul **(272 s)**

Chatzaras V, Dörr W, Finger F, Xypolias P, Zulauf G (2012) U–Pb single zircon ages and geochemistry of metagranitoid rocks in the Cycladic Blueschists (Evia Island): implications for the Triassic tectonic setting of Greece. Tectonophysics 595/596:125–139. doi:10.1016/j.tecto.2012.05.016

Delaloye M, Bingöl E (2000) Granitoids from western and northwestern Anatolia: geochemistry and modelling of geodynamic evolution. Geol Bull Turk 42:241–268

Fichtner A, Saygin E, Taymaz T, Cupillard P, Capdevillee Y, Trampert J (2013) The deep structure of the North Anatolian fault zone. Earth Planet Sci Lett 373:109–117

Fynn GW, Powell WFA (1979) The cutting and polishing of electro-optic materials. Adams Hilger, London

Genç ŞC, Yılmaz Y (1997) An example of post-collisional magmatism in northwestern Anatolia: the Kızderbent volcanics (Armutlu peninsula, Turkey). Turk J Earth Sci 6:33–42

Gözler MZ, Ergül E, Akçaören F, Genç S, Akat U, Acar S (1983) Çanakkale boğazı doğusu-Marmara Denizi güneyi-Bandırma-Balıkesir-Edremit ve Ege Denizi arasındaki alanını jeolojisi ve kompilasyonu, MTA Enstitüsü rapor no 7430, Ankara

Harris NBW, Kelley S, Okay AI (1994) Post-collisional magmatism and tectonics in northwest Anatolia. Contrib Miner Petrol 117:241–252

Harrison TM (1981) Diffusion of 40Ar in horn-blende. Contrib Miner Petrol 78:324–331

Harrison TM, Duncan J, McDougall J (1985) Diffusion of 40Ar in biotite. Temperature, pressure and composition effects. Geochim Cosmochim Acta 49:2461–2468

Hejl E, Bernroider M, Parlak O, Weingartner H (2010) Fission-track thermochronology, vertical kinematics and tectonic development along the western extension of the North Anatolian fault zone. J Geophys Res 115. doi:10.1029/2010JB007402

Hoeppener R (1955) Tektonik im Schiefergebirge. Geol Rundsch 44:26–58

Jolivet L, Brun JP (2008) Cenozoic geodynamic evolution of the Aegean. Int J Earth Sci. doi:10.1007/s00531-008-0366-4

Kahraman M, Cornwell DG, Thompson DA, Rost S, Houseman GA, Türkelli N, Teoman U, Poyraz SA, Utkucu M, Gülen L (2015) Crustal-scale shear zones and heterogeneous structure beneath the North Anatolian fault zone, Turkey, revealed by a high-density seismometer array. Earth Planet. Sci. Lett. 430:129–139

Karacık Z, Yılmaz Y, Pearce JA, Ece ÖI (2008) Petrochemistry of the South Marmara granitoids, northwest Anatolia, Turkey. Int J Earth Sci 97:1181–1200

Ketin İ (1946) Geological investigations in the Marmara Island and the Kapıdağ Peninsula (Marmara Adası ve Kapıdağ Yarımadası'nda jeolojik incelemeler). İU Sci Fac Bull Serie B XI 2:69–81 **(in Turkish)**

Kneuker T, Dörr W, Petschick R, Zulauf G (2014) Upper crustal emplacement and deformation of granitoids inside the Uppermost Unit of the Cretan nappe stack: constraints from U–Pb zircon dating, microfabrics and paleostress analyses. Int J Earth Sci. doi:10.1007/s00531-014-1088-4

Köprübaşı N, Aldanmaz E (2004) Geochemical constraints on the petrogenesis of Cenozoic I-type granitoids in northwestern Anatolia, Turkey: evidence for magma generation by lithospheric delamination in a post-collisional setting. Int Geol Rev 46:405–429

Le Pichon X, Kreemer C (2010) The Miocene-to-present kinematic evolution of the Eastern Mediterranean and Middle East and its implications for dynamics. Annu Rev Earth Planet Sci 38:323–351. doi:10.1146/annurev-earth-040809-152419

Martha SO, Dörr W, Gerdes A, Petschick R, Schastok J, Xypolias P, Zulauf G (2016) New structural and U–Pb zircon data from Anafi crystalline basement (Cyclades, Greece): constraints on the evolution of a Late Cretaceous magmatic arc in the Internal Hellenides. Int J Earth Sci (Geol Rundsch). doi:10.1007/s00531-016-1346-8

Okay AI (2008) Geology of Turkey: a synopsis. Anschnitt 21:19–42

Okay AI, Göncüoğlu MC (2004) The Karakaya Complex: a review of data and concepts. Turk J Earth Sci 13:77–95

Okay AI, Satır M (2000) Coeval plutonism and metamorphism in a latest Oligocene metamorphic core complex in northwest Turkey. Geol Mag 137(5):495–516

Okay AI, Tüysüz O (1999) Tethyan sutures of Northern Turkey. In: Durand B, Jolivet L, Horthváth F, Séranne M (eds) The Mediterranean Basin: tertiary extension within the Alpine Orogen: Geol Soc London, Special Publication, vol 156, pp 475–515

Okay AI, Satır M, Zattin M, Cavazza W, Topuz G (2008) An Oligocene ductile strike-slip shear zone: the Uludağ Massif, northwest Turkey—implications for the westward translation of Anatolia. GSA Bull 120:893–911

Passchier CW, Trouw RAJ (2005) Microtectonics. Springer, Berlin, p 366

Rockwell T, Ragona D, Seitz G, Langridge R, Aksoy M, Uçarkuş G, Ferry M, Meltzner A, Klinger Y, Meghraoui M, Satır D, Barka A, Akbalık B (2009) Palaeoseismology of the North Anatolian Fault near the Marmara Sea: implications for fault segmentation and seismic hazard. Geol Soc Lond 316:31

Sarıalioğlu S (1983) Kapıdağı Yarımadası'nda yeralan granodiyoritik plütonlar ve bunlara komşu kayaçların petrografi ve petrolojik etüdü. PhD Thesis. ITÜ Maden Fak. s. 92

Schmidt N-H, Olesen NO (1989) Computer-aided determination of crystal-lattice orientation from electron-channeling patterns in the SEM. Can Mineral 27:15–22

Şengör AMC, Yılmaz Y (1981) Tethyan evolution of Turkey: a plate tectonic approach. Tectonophysics 75:181–241

Şengör AMC, Tüysüz O, İmren C, Sakınç M, Eyidoğan H, Görür N, Le Pichon X, Rangin C (2005) The North Anatolian fault: a new look. Annu Rev Earth Planet Sci 33:37–112. doi:10.1146/annurev.earth.32.101802.120415

Twiss RJ (1977) Theory and applicability of a recrystallized grain size paleopiezometer. Pure Appl Geophys 115:225–244

Twiss RJ, Moores EM (1992) Structural geology. Freeman and Co, New York, p 532

Ulusoy U (2004) ESR dating of North Anatolian (Turkey) and Nojima (Japan) faults. Quat Sci Rev 23:161–174

Ustaömer PA, Ustaömer T, Collins AS, Reischpeitsch J (2009) Lutetian arc-type magmatism along the southern Eurasian margin: new U–Pb LA-ICPMS and whole-rock geochemical data from Marmara Island, NW Turkey. Miner Petrol 96:177–196

Uysal IT, Mutlu H, Altunel E, Karabacak V, Golding SD (2006) Clay mineralogical and isotopic (K–Ar, δ 18 O, δD) constraints on the evolution of the North Anatolian fault zone, Turkey. Earth Planet Sci Lett 243:181–194. doi:10.1016/j.epsl.2005.12.025

Yılmaz Y, Tüysüz O, Yiğitbaş E, Genç ŞC, Şengör AMC (1997) Geology and tectonic evolution of the Pontides. In: Robinson AG (ed) Regional and petroleum geology of the black sea and surrounding region: American Association of Petroleum Geologists, Memoir, vol 68, pp 183–226

Zattin M, Okay AI, Cavazza W (2005) Fission track evidence for late Oligocene and mid-Miocene activity along the North Anatolian fault in southwestern Thrace. Terra Nova 17:95–101. doi:10.1111/j.1365-3121.2004.00583.x

Zulauf G (2001) Structural style, deformation mechanisms and paleostress along an exposed crustal section: constraints on the rheology of quartzofeldspathic rocks at supra- and infrastructural levels (Tepla Barrandian unit, Bohemian Massif). Tectonophysics 332:211–237